Holistic Efficiency Map Calculation of Variable Flux Machines Regarding Relative Magnetisation

Julius Kesten
Institute of Electrical Engineering
Karlsruhe Institute of Technology
Karlsruhe, Germany
julius.kesten@kit.edu

Philipp Müller
Insitute of Sustainable Energy Systems
Offenburg University of Applied Sciences
Offenburg, Germany
philipp.mueller@hs-offenburg.de

Matthias Brodatzki
Institute of Electrical Engineering
Karlsruhe Institute of Technology
Karlsruhe, Germany
brodatzki@kit.edu

Martin Doppelbauer
Institute of Electrical Engineering
Karlsruhe Institute of Technology
Karlsruhe, Germany
martin.doppelbauer@kit.edu

***Abstract*—An algorithm for the integral calculation of efficiency maps of variable flux machines under consideration of the relative flux level is presented. The general idea and the algorithm logic are presented in detail and the efficiency map calculation is validated against a conventional gradient based efficiency map calculation algorithm. Instead of calculating efficiency maps for discrete flux levels and interpolating these maps afterwards, the algorithm presented here directly includes the relative magnet flux in the efficiency calculation. The presented approach uses torque and voltage surfaces in a plane of current, current angle and flux level. As results, the an exemplary efficiency map calculated with the algorithm is presented and the effect of different numbers of underlying data sets are discussed. Finally, a short outlook on practical applications is given.**

***Index Terms*—variable flux machine, optimization algorithm, efficiency, flux level**

I. Introduction

Variable flux machines (VFM) have been discussed as an alternative to rare earth magnet synchronous machines (permanent magnet synchronous machines - PSM). This machine type typically employs the low coercive fields of AlNiCo permanent magnets (PM) to allow control of the rotor's excitation during operation, eliminating the need for permanent d-current field weakening and thus increasing a machine's efficiency in the field weakening range. [1], [2], [3]
During the design process of VFM, two parameters have to be regarded in addition to those considered for the design of regular PSM. The first of these are the external fields acting on the magnets during "normal", i.e. operation without any change of magnetisation state. Secondly, the optimum flux level in terms of efficiency for each working point in the speed-torque-plane needs to be considered. The first of these restrictions was investigated and methods for its mitigation were presented. Here, the number of points in a discrete flux map acquired through FEA simulations for which the actual external fields exceed the permissible value are used as nonlinear boundary in an optimisation process. [4]
Further design considerations for VMF include coupled models utilising magnetic equivalent circuits and mechanical models based on differential algebraic equations to describe the effect of magnetisation state changes on the machine's NVH behaviour. This approach presented in [5] allows the consideration of the NVH characteristics early in the design process. General guidelines considering the design of VFM were discussed in [6] where the focus lay on establishing a parameter plane, similar to the one presented in [7], assessing the effectiveness of reducing the PM flux in the field weakening range in terms of efficiency gains. Further, design methodologies were presented to specifically meet traction requirements in terms of inverter sizing and power delivery across the speed range of the machine [8], utilising so called hybrid magnet arrangements.
VFM employing this topology use two different types of magnets, one low coercive field one, typically AlNiCo, and the other a high coercive field one, mostly NdFeB alloys. By arranging the two magnet systems either in series or parallel, different advantages can be achieved, such as reduced d-current amplitudes for magnetisation and less simple demagnetisation in series configurations or easier demagnetisation and higher output flux in parallel magnetisation. [8], [9]
Also, the losses occuring while changing the magnetisation state were analysed in the authors' previous work, allowing to incorporate this knowledge in cycle efficiency calculations. [10]
All of the works mentioned above present guidelines or design principles for VFM. However, the effect of the varying rotor flux on the machines' characteristics is regarded mostly by interpolation of efficiency maps recorded at different discrete flux levels. These maps are typically computed using η-optimisation algorithms or the MTPA strategy, meaning a complete optimisation is carried out for each discrete flux level

This work was part of the research project "ReMos2" ("Reluktanzmaschine für effiziente Mobilität ohne seltene Erden 2"), financed through the Ministry of Science, Research, and Arts of the Federal State of Baden-Württemberg in the framework of "Innovationscampus Mobilität der Zukunft".

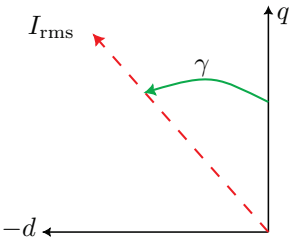

Fig. 1: Current phasor I_{rms} (red, dashed) and current angle γ (green) in the dq-plane

before the interpolation takes place. This approach requires time and computational ressources. Therefore, an optimisation algorithm incorporating the rotor flux as additional degree of freedom in the optimisation process is presented in this work, allowing the computation of efficiency maps with regard to the optimal flux level across a machine's entire operating range. Thus, the interpolation is mitigated and the computation becomes more efficient. In section II the basic idea and the functionality of the algorithm are presented and discussed. Subsequently, in section III, the integration for the calculation of efficiency maps using this algorithm is discussed. The performance of the presented method is put in perspective through a comparison with an optimisation tool chain in section IV. Finally, a conclusion and an outlook are given in section V.

II. Holistic Efficiency Optimisation

A. General idea

The proposed algorithm is based on a spatial interpretation of the parameters of interest. The current I_{rms}, the current angle γ and the flux level in the machine $\Psi_{\%}$ represent a three dimensional plane, in which surfaces of constant inner torque can be placed. The angle γ represents the angle between the q-axis and the current phasor in the dq-plane as is presented in Fig. 1. The concept of the three-parameter-plane is illustrated in Fig. 2, where the first of the two surfaces represents the constant torque one. The second surface (blue) represents the voltage limit for the investigated working point and each of the I-γ-Ψ-combinations presented in the figure. The colour map of the torque surface represents the efficiency for each of the combinations, illustrating that the same inner torque can be achieved with an infinite amount of constellations of these parameters, each yielding different machine efficiencies. To find the optimal – being the most efficient one – combination of the I-γ-Ψ-triple, the point with the best efficiency on the torque surface that does not violate the voltage limit needs be found. In order to generate the well-known efficiency maps in the torque-speed-plane this process is iterated for every working point of interest.

The data which these calculations are performed on consists flux maps generated using 2D FEA analyses for one given speed n. Further, loss maps are available in order to determine the efficiency of the respective working points. All data exists

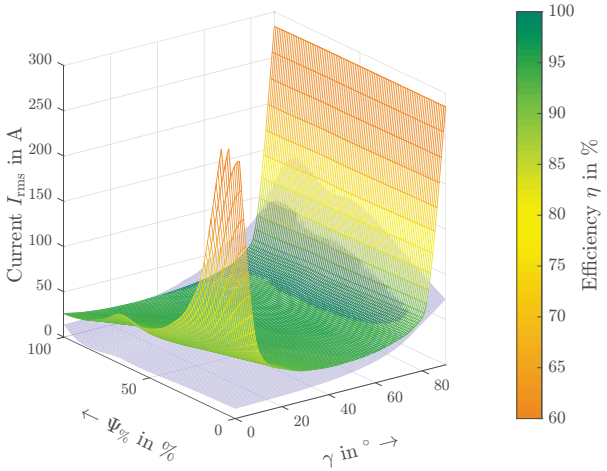

Fig. 2: Constant-torque-surface, voltage limit represented by blue surface

dependent of the current I_{rms} and the current angle γ, while each set of those maps also exists for each flux level $\Psi_{\%}$ simulated. To generate the constant torque surface as shown above, the formulas for the steady state inner torque and the voltage are applied.

$$\underline{\mathbf{T}} = \frac{3}{2}\left(\underline{\boldsymbol{\Psi}}_{\mathrm{q}} \circ \underline{\mathbf{I}}_{\mathrm{d}} - \underline{\boldsymbol{\Psi}}_{\mathrm{d}} \circ \underline{\mathbf{I}}_{\mathrm{q}}\right) \tag{1}$$

$$\underline{\mathbf{U}}_{\mathrm{d}} = R_{\mathrm{s}} \cdot \underline{\mathbf{I}}_{\mathrm{d}} - \omega_{\mathrm{el}}\left(\underline{\boldsymbol{\Psi}}_{\mathrm{q}} + L_{\mathrm{wh}} \cdot \underline{\mathbf{I}}_{\mathrm{q}}\right) \tag{2}$$

$$\underline{\mathbf{U}}_{\mathrm{q}} = R_{\mathrm{s}} \cdot \underline{\mathbf{I}}_{\mathrm{q}} + \omega_{\mathrm{el}}\left(\underline{\boldsymbol{\Psi}}_{\mathrm{d}} + L_{\mathrm{wh}} \cdot \underline{\mathbf{I}}_{\mathrm{d}}\right) \tag{3}$$

$$\hat{\underline{\mathbf{U}}} = \sqrt{\underline{\mathbf{U}}_{\mathrm{d}} \circ \underline{\mathbf{U}}_{\mathrm{d}} + \underline{\mathbf{U}}_{\mathrm{q}} \circ \underline{\mathbf{U}}_{\mathrm{q}}}, \tag{4}$$

Here, the d- and q-current components $\underline{\mathbf{I}}_{\mathrm{d}}$ and $\underline{\mathbf{I}}_{\mathrm{q}}$ as well as the respective flux components $\underline{\boldsymbol{\Psi}}_{\mathrm{d}}$ and $\underline{\boldsymbol{\Psi}}_{\mathrm{q}}$ are represented as tensors, as are the electromagnetic torque $\underline{\mathbf{T}}$ and the voltage components $\underline{\mathbf{U}}_{\mathrm{d}}$ and $\underline{\mathbf{U}}_{\mathrm{q}}$ and the voltage amplitude $\hat{\underline{\mathbf{U}}}$. This representation is selected to highlight the multi-dimensionality of this data, with $I_{\mathrm{rms}} \times \gamma$ dimensions. The stator's winding resistance R_{S}, the estimated winding head inductance L_{wh} and the electrical angular frequency ω_{el}, however, are scalar. In addition to the calculations above, the loss maps are adjusted to match the considered speed and torque working points using Bertotti's model [11]. Other losses, such as joule or windage losses are calculated analytically for the desired working points.

B. Algorithm execution

The single steps of which the algorithm consists are put in context in Fig. 3. During the step denoted as *Initialisation* the algorithm execution is prepared: The working points (torque and speed) to be considered are defined and the underlying FEA data is prepared. For example, the iron loss maps are scaled. In a further step during the *Initialisation* node, the initial search area for the free parameters $\Psi_{\%}$ and γ is set by initially assigning the length $||\boldsymbol{\Psi}_{\%\mathrm{search}}||_{\ell}$ and $||\boldsymbol{\gamma}_{\mathrm{search}}||_{\ell}$ of the search vectors $\boldsymbol{\Psi}_{\%\mathrm{search}}$ and $\boldsymbol{\gamma}_{\mathrm{search}}$ and initialising them with starting values. These typically are $\gamma_{\mathrm{min}} = 0°, \gamma_{\mathrm{max}} =$

$90°$ and $\Psi_{\%,\min} = 0\,\%, \Psi_{\%,\max} = 100\,\%$.
The variable k denotes the number of iterations done for the main part of the algorithm, which is represented by the dash-dotted line in Fig. 3. The variables i and j represent the control variables for the steps in the $\boldsymbol{\Psi}_{\%\text{search}}$ and $\boldsymbol{\gamma}_{\text{search}}$ vectors, respectively. Using both these vectors, the current values I_{rms} that allow the production of a desired inner torque T_{w} are determined by solving for $I_{\text{rms}}|_{\text{T}_\text{w}}$ the equation

$$0 = \underbrace{f(I_{\text{rms}}|_{T\text{W}}, \gamma, \Psi_{\%})}_{\bar{T}_{\text{w}}} - T_{\text{w}} \tag{5}$$

for $i \times j$ iterations, thereby regarding all combinations of relative flux $\Psi_{\%}$ and current angle γ. The voltage limit can be represented as

$$0 = \underbrace{f(I_{\text{rms}}|_{\hat{\text{U}}}, \gamma, \Psi_{\%})}_{\bar{U}_{\max}} - U_{\max} \tag{6}$$

and yields a maximum permitted current $I_{\text{rms}}|_{\hat{\text{U}}}$ for the same $i \times j$ combinations as above. The variables with the $\bar{}$ symbol denote the interpolation of the respective quantities using the current I_{rms}, the current angle γ and the relative PM flux $\Psi_{\%}$. The calculations for both the current $I_{\text{rms}}|_{\text{T}_\text{w}}$ and the current $I_{\text{rms}}|_{\hat{\text{U}}}$ take place during execution of the node labeled *Torque and voltage surface calculation* and represent the surfaces introduced in the previous section II-A.
After both surfaces were calculated, a comparison of whether there is any entry in the resulting current matrix that satisfies the condition

$$I_{\text{ij,k}}|_{\text{T}_\text{w}} \leq I_{\text{ij,k}}|_{\hat{\text{U}}} \tag{7}$$

is performed in the step *Legality check*. If such an entry is found, it is labeled as legal by means of a search mask $\mathbf{Q}_{\text{k}}$. This matrix is of the dimension $i \times j$ as well and thus represents every γ-$\Psi_{\%}$-combination for which a given current can be applied to produce the desired torque T_{w} without exceeding

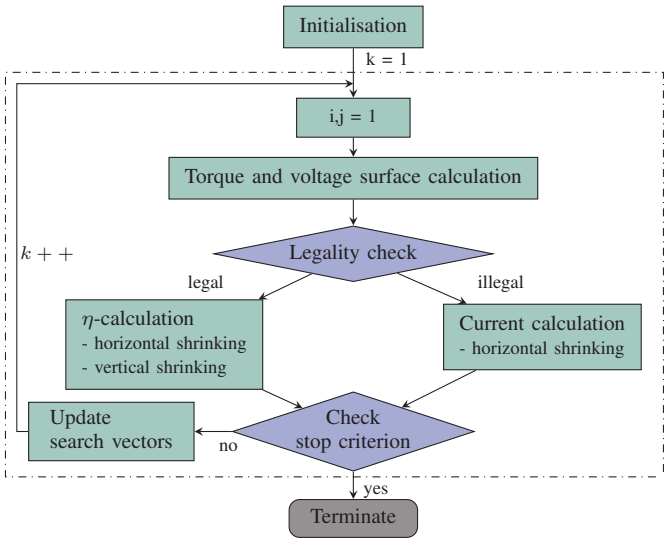

Fig. 3: Holistic optimisation algorithm flow chart

the voltage limit in the current iteration k of the algorithm.
In case of one or more legal entries, i.e. one or more values $q_{\text{ij,k}} = 1 \exists i, j$, the node *$\eta$-calculation* is activated, where the highest efficiency is selected and written into a vector $\tilde{\boldsymbol{\eta}}(k)$. Similarly, the current, current angle and relative flux are saved to the respective vectors

$$\tilde{\boldsymbol{\eta}}(k) = \tilde{\eta}_{\text{k}} \tag{8}$$

$$\tilde{\mathbf{I}}(k) = \mathbf{I}_{\text{k}}|_{\text{T}_\text{w}}(\tilde{i}, \tilde{j}) \tag{9}$$

$$\tilde{\boldsymbol{\gamma}}(k) = \gamma_{\text{search,k}}(\tilde{i}, \tilde{j}) \tag{10}$$

$$\tilde{\boldsymbol{\Psi}}_{\%}(k) = \Psi_{\%,\text{search,k}}(\tilde{i}, \tilde{j}), \tag{11}$$

where the $\tilde{}$ symbol denotes the optimum values of the quantities for the step k. Note that while $\tilde{\mathbf{I}}$, $\tilde{\boldsymbol{\gamma}}$ and $\tilde{\boldsymbol{\Psi}}_{\%}$ all depend on the combination of γ and $\Psi_{\%}$, the efficiency $\tilde{\boldsymbol{\eta}}$ is solely dependent on the iteration variable k. To self validate the algorithm's results after each iteration k, the torque and voltage values T_{k} and $\hat{U}_{\text{k}}$ are calculated from the optimum values presented above, instead of assigning the desired torque T_{w} or the voltage limit $U_{\max}$. This ensures correct solutions for (5) and (6).
After these preliminary optima were recorded, the algorithm then adapts the limits of the search vectors $\boldsymbol{\gamma}_{\text{search}}$ and $\boldsymbol{\Psi}_{\%\text{search}}$, while keeping their lengths $||\boldsymbol{\Psi}_{\%\text{search}}||_\ell$ and $||\boldsymbol{\gamma}_{\text{search}}||_\ell$ constant. This "shrinking" of the search area – which applies to the different maps introduced in section II-A – is conducted in two steps: first a "horizontal" one along the dimension of $\boldsymbol{\gamma}_{\text{search}}$ and secondly a "vertical" one along the dimension of $\boldsymbol{\Psi}_{\%\text{search}}$. For the horizontal shrinking, the column $\tilde{j}$, containing $\tilde{\eta}_{\text{k}}$ is selected. If $\tilde{j} \geq 2$ and $\tilde{j} \leq ||\boldsymbol{\gamma}_{\text{search}}||_\ell - 1$ hold, the new limits of the search area, i.e. $\gamma_{\max,\text{k}}$ and $\gamma_{\min,\text{k}}$, are selected to include the γ-values of the two neighbouring columns $\tilde{j}+1$ and $\tilde{j}-1$. If $\tilde{j}$ lies in the outer columns to either side of the matrix, only one neighbouring column is included, respectively.
The goal of the vertical shrinking is the removal of rows containing NaN entries only. After exclusion of these rows the remaining search area, i.e. the interval between $\Psi_{\%,\max,\text{k}}$ and $\Psi_{\%,\min,\text{k}}$, includes the maximum efficiency $\tilde{\eta}_{\text{k}}$ of the current iteration k.
If however, the condition from (7) is not satisfied for the current iteration step, the *Current calculation* is performed. In this part of the process, it is not an optimal efficiency that is sought after, but the γ-$\Psi_{\%}$ combination yielding the smallest difference between that current magnitude which can be used to reach T_{w} and the one necessary to satisfy the condition (7). Applied to the image of the surfaces as in Fig. 2, this means looking for the point where the torque and the voltage surface are closest to each other given as

$$\boldsymbol{\Delta I_{\text{k}}} = \left|\mathbf{I}_{\text{k}}|_{\text{M}_\text{w}} - \mathbf{I}_{\text{k}}|_{\hat{\text{U}}}\right| \tag{12}$$

$$\widetilde{\Delta I}_{\text{k}} = \boldsymbol{\Delta I_{\text{k}}}(\tilde{i}, \tilde{j}) = \min\left(\boldsymbol{\Delta I_{\text{k}}}\right). \tag{13}$$

Here $\widetilde{\Delta I}_{\text{k}}$ represents the current magnitude with the smallest distance between both surfaces as the "optimum" value. However, the corresponding efficiency η is not transferred into the

result vector $\tilde{\boldsymbol{\eta}}$ with its actual value, but as a NaN to record the infeasibility of this result. The other values are saved to the respective vectors as they are. In a subsequent step, the search is focused on the area around $\widetilde{\Delta I}_{\mathrm{k}}$ with improved resolution through the horizontal shrinking described above. This opens the possibility to find a small legal area for which (7) is met and that was overseen with the coarser grid.

These steps in the main (dash-dotted) part are repeated k times until either a maximum number of repetitions $k_{\max}$ is reached, the desired residual

$$\epsilon > |\tilde{\boldsymbol{\eta}}\,(k-1) - \tilde{\boldsymbol{\eta}}(k)| \tag{14}$$

is achieved or the efficiency can not be calculated any further. This is the case, if in two subsequent steps k the efficiency $\tilde{\eta}_{\mathrm{k}}$ is NaN. The reason for this is either the lack of an intersection between the torque and voltage surfaces, while both of them may be viable, or because the desired torque T_{w} cannot be achieved with the permitted maximum current $I_{\max}$. This step is represented through the node *Check stop criterion* in Fig. 3. If the execution is terminated, the respective kth values of (8) - (11) are regarded as the optima. If, however, none of the stop criteria apply, execution continues through the node *Update search vectors*. Here, the new values for $\gamma_{\max,\mathrm{k}+1}$, $\gamma_{\min,\mathrm{k}+1}$, $\Psi_{\%\max,\mathrm{k}+1}$ and $\Psi_{\%\min,\mathrm{k}+1}$ for the next iteration step $k+1$ are applied and the data within the new limits is divided into the $||\boldsymbol{\Psi}_{\%\mathrm{search}}||_\ell$ and $||\boldsymbol{\gamma}_{\mathrm{search}}||_\ell$ steps.

III. Calculation of Effciency Maps

A. Overview

The holistitc algorithm presented in the previous section allows the determination of the best η, considering I_{rms}, γ, as well as the magnetisation level $\Psi_{\%}$, for a given speed n and torque T_{w}. To gain the desired efficiency and other performance maps of the machine, the algorithm is embedded in the procedure shown in Fig. 4. First, the speed sampling points $\mathbf{n}_{\mathrm{s}}$ and the length $||\mathbf{t}_{\mathrm{s}}||_\ell$ of the torque sampling vectors are defined in the *Initialisation* step and both iteration variables are initalised: $i = 1$, $j = 1$. After setting these initial variables, iteration over the j speed sampling points begins. The actual values for the torque sampling points are calculated dynamically depending on the maximum torque found during the *Torque-speed-envelope calculation*. This calculation is based on the holistic optimisation algorithm: The torque matrix including all entries for the given speed n_{j} is calculated and compared to the voltage limitation. Should the largest entry of the matrix stay within the limit, it is accepted as the maximum torque for the given speed. Else, the entry in the torque matrix with the largest value respecting the boundary is selected. This step is executed for every entry j in the speed vector $\mathbf{n}_{\mathrm{s}}$, meaning the torque-speed-envelope is calculated piece-wise.

After the partial envelope was calculated, the first torque sampling point $\mathbf{t}_{\mathrm{s}}|_{\mathrm{n_j}}(i)$ is regarded and used as desired torque T_{w} for the execution of the *Holistic optimisation*, which yields the current, current angle, and flux level to achieve T_{w} at maximum efficiency. The results of the algorithm execution are stored in the *Save data* step and the torque's iteration variable i is increased by 1, until the maximum torque for the current speed n_{j} is reached ($i = ||\mathbf{t}_{\mathrm{s}}||_\ell$). This part of the algorithm then yields a vector with a number of $||\mathbf{t}_{\mathrm{s}}||_\ell$ torque sampling points for the given speed step n_{j}. The outer loop considers the speed sampling points $\mathbf{n}_{\mathrm{s}}$. After all data points were considered, such maps as the losses, the current's and flux' dq-components or the power factor are calculated in the step *Calculation of additional maps*. Upon reaching the *Terminate* node, the machine's characteristics are completely defined for the $m_{\mathrm{s}} \times n_{\mathrm{s}}$ plane.

IV. Calculation Results and Comparison With Conventional Method

A. Machine under investigation

The machine considered for the results presented in this section is a 6 pole VFM with a large portion of reluctance torque. It employs 36 stator slots with hairpin windings. The main features of the machine are summarised in Table I, its cross section is presented in Fig. 5. The magnet material is the AlNiCo alloy LNGT80, with a remnant flux density $B_{\mathrm{rem}} = 1.05\,\mathrm{T}$ and a coercivity $H_{\mathrm{c}} = 119\,\mathrm{kA/m}$. The simulation results were recorded using Ansys Electronics and the algorithm is implemented in MATLAB.

B. Validation of the holistic optimisation

The proposed algorithm is validated by comparison to a conventional design toolchain based on η-optimisation via gradient based optimisers. To enable a direct comparison, the holistic algorithm is executed with FEA data employing one

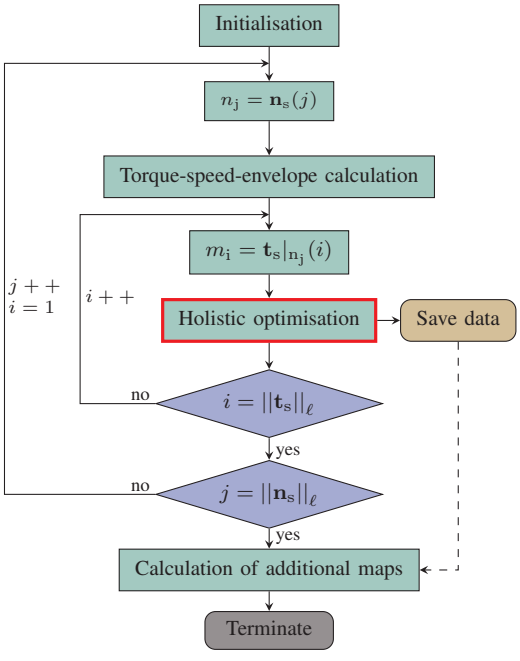

Fig. 4: Efficiency map creation flow chart

TABLE I: Characteristics of the machine under investigation

Characteristic	Value
No. of phases m	3
No. of pole pairs p	3
No. of slots N_s	36
No. of conductors per coil Z_c	4
Stator bore diameter D_b (mm)	140
Electric sheet material	NO-30
Maximum current (A)	300
DC link Voltage (V)	400

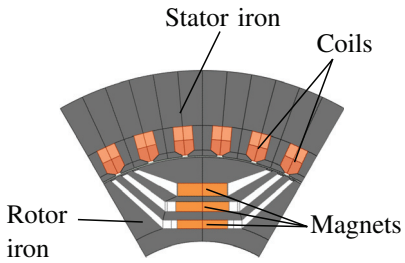

Fig. 5: Cross-section of the machine under investigation

magnetisation state only. To ensure a proper comparison, two data sets are regarded individually: one with a magnetisation level $\Psi_\% = 50\,\%$ and one with $\Psi_\% = 100\,\%$. Fig. 6 presents the results of this comparison, where the colour maps show the error between the absolute value of both results as in (15):

$$\Delta\eta\left(n_\mathrm{s}, m_\mathrm{s}\right) = \left|\tilde{\eta}_\mathrm{conv}\left(n_\mathrm{s}, m_\mathrm{s}\right)|_{\Psi_\%} - \tilde{\eta}_\mathrm{hol}\left(n_\mathrm{s}, m_\mathrm{s}\right)|_{\Psi_\%}\right| \tag{15}$$

where $\tilde{\eta}_\mathrm{conv}$ is the result of the conventional post processing and $\tilde{\eta}_\mathrm{hol}$ is the result employing the holistic algorithm. To ensure proper comparability, the speed sampling vectors $\mathbf{n}_\mathrm{s}$ were selected to be equal. The torque sampling vectors $\mathbf{m}_\mathrm{s}$ differ according to the dynamic sampling point definition of the holistic algorithm described in section III. For both optimisers, the residual was selected to be $\epsilon = 0.05$, meaning differences between both results up to this magnitude are negligible. The length of both search vectors $||\mathbf{\Psi}_{\%\mathrm{search}}||_\ell$ and $||\boldsymbol{\gamma}_\mathrm{search}||_\ell$ was set to 11 for these and all subsequent results. Overall, the results show good agreement between both approaches. With the computer setup used, the holistic optimiser requires about one quarter of the time to complete the efficiency map calculation compared to the conventional algorithm.

C. Holistic optimisation results

The main goal of the holistic opimisation approach is to calculate efficiency maps under regard of the flux level $\Psi_\%$. The amount of FEA data sets with different flux levels is fundamental for the quality of the resulting maps. Therefore, the resulting maps are presented for two datasets of different size, namely a large data set D_l with nine entries, and a medium one D_m with five entries, to compare the execution

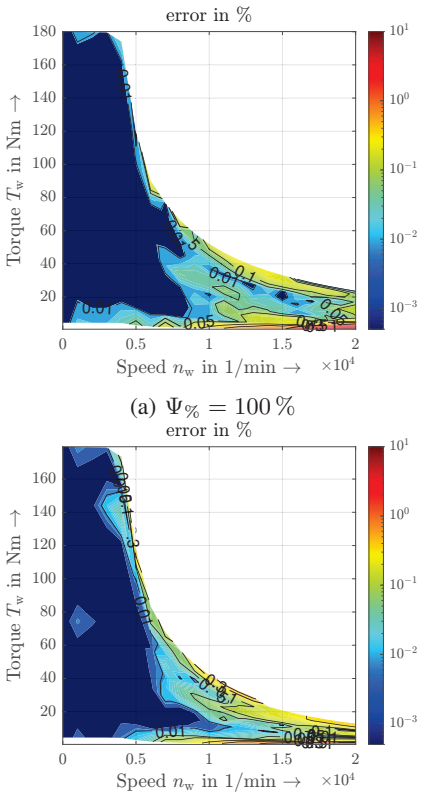

(a) $\Psi_\% = 100\,\%$

(b) $\Psi_\% = 50\,\%$

Fig. 6: Percentage error between the holistic optimisation and the conventional approach for two flux levels $\Psi_\% = 50\,\%$ and $\Psi_\% = 100\,\%$

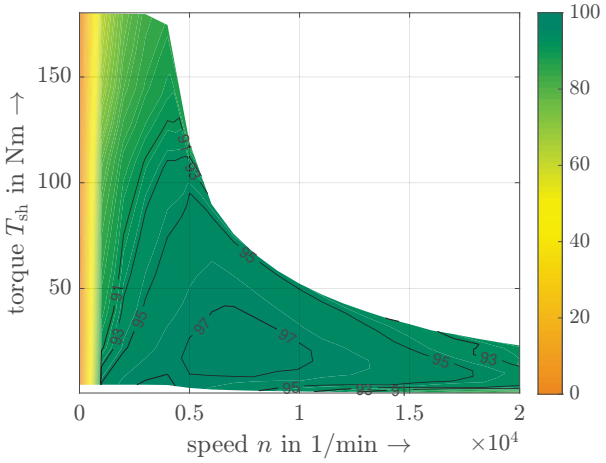

Fig. 7: Calculated efficiency map for optimised flux levels $\Psi_\%$

times and the results. The corresponding flux levels simulated in FEA are the following:

$$\Psi_{\%,\mathrm{b}} = [100\,\%, 95\,\%, 85\,\%, 80\,\%, 75\,\%, 50\,\%, 25\,\%, 0\,\%]$$
$$\Psi_{\%,\mathrm{m}} = [100\,\%, 75\,\%, 50\,\%, 25\,\%, 0\,\%]$$

The choice of data points in D_l especially was done based on previous knowledge of the investigated machine, as presented

in section IV-A, where the main effect of flux reduction was found for flux levels above $50\,\%$. A complete efficiency map, that was calculated using D_l, is presented in Fig. 7 to give a complete representation of the machine's characteristics. Here T_sh represents the machine's mechanical shaft torque, which regards the losses. The results for the optimal flux and the efficiency gain for both datasets are presented Fig. 8. As becomes visible in comparison of both figures, the differences between the calculation results are small. However, due to the higher resolution of D_l especially in the area of $\Psi_\%$ between $100\,\%$ and $50\,\%$ it is valid to assume that the results of the bigger data set give a better representation of the optimum flux levels. The main effect of the variable magnetisation is visible for high speeds under partial load. Due to the machine's geometry there is a large portion of reluctance torque of about $80\,\%$. Therefore, a derating of the magnets impacts efficiency only to a certain degree, as the contribution to torque generation becomes negligible for $\Psi_\% < 50\,\%$, since the magnets' output flux is small at this point. This, in turn, means there is sufficiently little d-current required during stationary operation to weaken the magnet flux Ψ_PM, meaning a further "permanent" demagnetisation would have no beneficial effect on the machine's efficiency. While the results gathered with data set D_l may be more precise, they also require $25\,\%$ more computational time than those of D_m. During the investigations into the holistic algorithm, a small data set D_s consisting of only two magnetisation levels $\Psi_{\%,\mathrm{s}} = [100\,\%, 0\,\%]$ was regarded also. The results of this data set have little representative value and are therefore omitted in this paper.

V. Conclusion and Outlook

An algorithm for the integrated efficiency map calculation of variable flux machines based on a windowed search on torque and voltage surfaces was presented. The single steps of the algorithm were presented for the calculation of a single working point and subsequently the integration into the efficiency map calculation is described. The presented algorithm was tested against a conventional, i.e. gradient based, efficiency map calculation algorithm and showed a four-fold increase in performance. After the comparison proved the feasibility of the proposed approach, the results of the integrated calculations were presented.

In a next step, the generated results need be compared to measurement data for further validation. This would prove the feasibility of the algorithm for the prediction of the stationary behaviour of VFM. Once this validation is completed successfully, the presented approach itself may be used to validate analytical models of VFM. Also, with the ability to efficiently interpolate data from discrete flux levels, test bench measurements can be processed as well. For this application, the dynamic search can be modified, so that measurements with one specific flux level only need to be carried out in those parts of the machine's performance range for which the respective flux level is expected to achieve efficiency improvements.

At this point, the algorithm generating the efficiency maps is executed serially. An implementation allowing parallel computation of the torque speed working points would allow faster computation, since these calculations take place independently. The core functionality of the holistic optimiser also allows the calculation of cycle efficiencies of the variable flux machines. To do so, the torque and speed sampling points supplied to the algorithm need to be the cycle working points. Utilising this feature it is then possible to examine the efficiency of a VFM compared to a conventional PSM under different boundary conditions imposed by restricting the number of state changes by using a hysteresis based flux level controller.

Since the choice of the third parameter in the presented plane is not limited to the permanent magnet flux, the algorithm can also be adapted for use with externally excited machines or to include thermal restrictions in the design process.

References

[1] V. Ostovic, "Memory motors," *IEEE Industry Applications Magazine*, vol. 9, no. 1, pp. 52–61, Jan. 2003.

[2] R. Jayarajan, N. Fernando, and I. U. Nutkani, "A Review on Variable Flux Machine Technology: Topologies, Control Strategies and Magnetic Materials," *IEEE Access*, vol. 7, pp. 70 141–70 156, 2019. [Online]. Available: https://ieeexplore.ieee.org/document/8721627/

[3] K. Sakai, K. Yuki, Y. Hashiba, N. Takahashi, and K. Yasui, "Principle of the variable-magnetic-force memory motor," in *2009 International Conference on Electrical Machines and Systems*. IEEE, 2009, pp. 1–6.

[4] J. Kesten, F. Frölich, F. Wittemann, J. Knirsch, F. Bechler, L. Kärger, P. Eberhard, F. Henning, and M. Doppelbauer, "Design Approach for a Novel Multi Material Variable Flux Synchronous Reluctance Machine without Rare Earth Magnets," in *2022 International Conference on Electrical Machines (ICEM)*. IEEE, 2022, pp. 2304–2310.

[5] F. Bechler, J. Kesten, F. Wittemann, F. Henning, M. Doppelbauer, and P. Eberhard, "Simplified modeling of electromagnets for dynamic simulation of transient effects for a synchronous electric motor," *International Journal of Mechanical System Dynamics*, vol. 1, no. 1, pp. 89–95, Jan. 2021.

[6] B. Gagas, T. Fukushige, N. Limsuwan, C.-Y. Yu, K. Akatsu, and R. D. Lorenz, "Suggested design space in a PMSM parameter plane for variable flux machines," in *2013 International Electric Machines & Drives Conference*. IEEE, May 2013, pp. 549–556.

[7] W. Soong, "Field-weakening performance of brushless synchronous AC motor drives," *IEE Proceedings - Electric Power Applications*, vol. 141, no. 6, p. 331, 1994.

[8] A. Athavale, K. Sasaki, B. S. Gagas, T. Kato, and R. D. Lorenz, "Variable Flux Permanent Magnet Synchronous Machine (VF-PMSM) Design Methodologies to Meet Electric Vehicle Traction Requirements with Reduced Losses," *IEEE Transactions on Industry Applications*, vol. 53, no. 5, pp. 4318–4326, Jan. 2017.

[9] M. Ibrahim and P. Pillay, "Design of Hybrid Variable Flux Motors for Enhanced Wide-Speed Performance," in *2019 IEEE Energy Conversion Congress and Exposition (ECCE)*. IEEE, Sep. 2019, pp. 6046–6053.

[10] J. Kesten and M. Doppelbauer, "Quick Prediction of Losses During Magnetization State Changes in Variable Flux Machines," in *2023 IEEE International Electric Machines & Drives Conference (IEMDC)*. San Francisco, CA, USA: IEEE, May 2023, pp. 1–7. [Online]. Available: https://ieeexplore.ieee.org/document/10238851/

[11] G. Bertotti, "General properties of power losses in soft ferromagnetic materials," *IEEE Transactions on Magnetics*, vol. 24, no. 1, pp. 621–630, Jan. 1988.

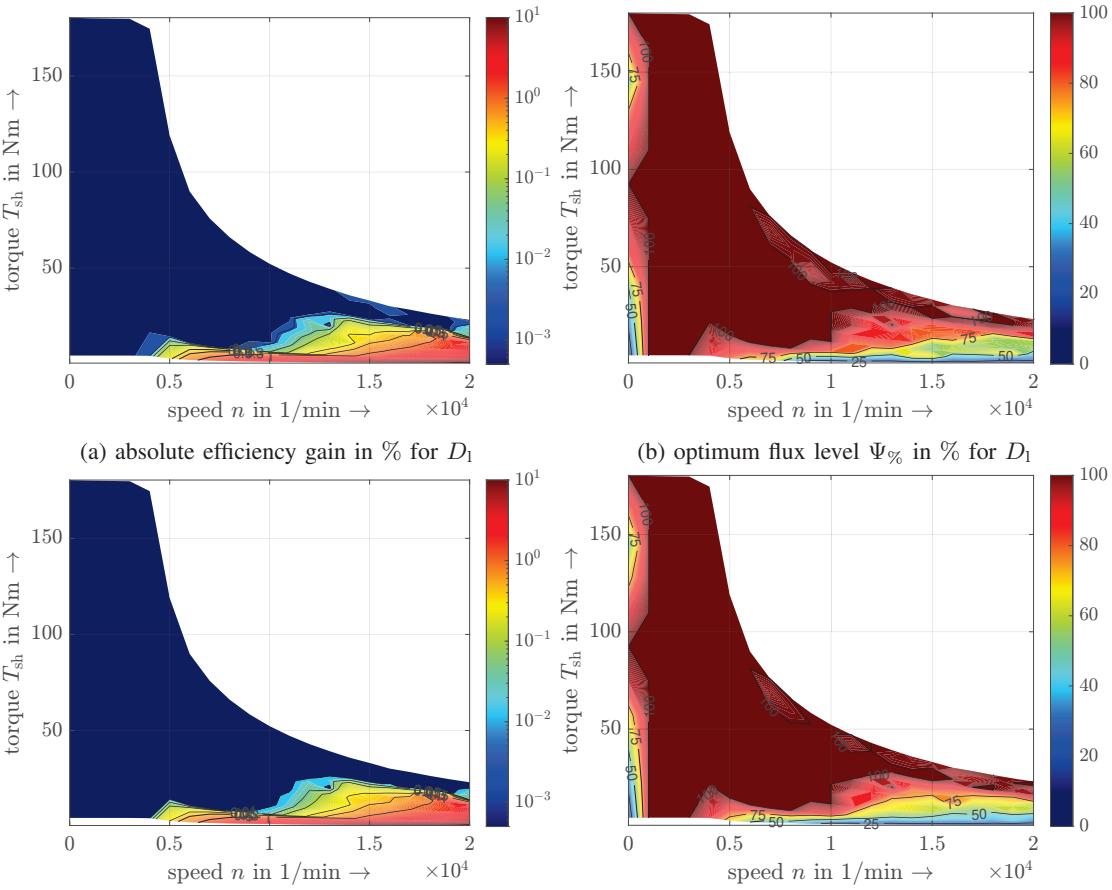

(a) absolute efficiency gain in % for D_{l}

(b) optimum flux level $\Psi_{\%}$ in % for D_{l}

(c) absolute efficiency gain in % for D_{m}

(d) optimum flux level $\Psi_{\%}$ in % D_{m}

Fig. 8: Efficiency gain and optimum flux level for both datasets